A Numerical Investigation on Active Chilled Beams for Indoor Air Conditioning

Cammarata G., Petrone G.*

Department of Industrial and Mechanical Engineering, University of Catania
Viale Andrea Doria 6 – 95125 Catania, ITALY
*Corresponding author: gpetrone@diim.unict.it

Abstract: In this study fluid-dynamical and thermal performance of active chilled beams is investigated by 2D and 3D modelling in COMSOL Multiphysics. Three different typologies of those air conditioning systems are considered. Results, obtained for typical range of variation of operational conditions, are principally produced as temperature and velocity distributions. Special attention is paid to the evaluation of indicative parameters of comfort for human occupants, like maximum value of velocity airflow in the occupied portion of the room and horizontal and vertical temperature gradient. Dynamical and thermal efficiency are also analysed by monitoring key functional parameters for active chilled beams both in winter and summer season applications.

Keywords: Ventilation of buildings, ceiling systems, heat transfer, turbulent flow.

1. Introduction

In the modern society, people spend more than 90% of their time in an artificial environment, for instance inside buildings [1-2]. For this reason studies concerning indoor air quality and thermal comfort for occupants of conditioned environment are arguments of very actual interest. A great part of studies present in literature on this subject are experimentally conducted. However, during the last few years more and more interest has been paid to the CFD approach for predicting air flows in ventilated rooms [3]. In the present study the FEM based software COMSOL Multiphysics is exploited for simulating air flow in rooms ventilated by a particular ceiling air distribution system called chilled beams. Chilled beams are air conditioning systems that combine fresh air supplying with indoor cooling or heating. The functional principle (Figure 1) of that system consists in aspiration of air room inside the ceiling conditioning component caused by an high velocity jet supplying external fresh air. Inducted air room is re-circulated into the beam and forced to flow through a water-air heat exchanger where it is cooled or heated. Then it is mixed with the fresh air and so it is introduced in the room from diffusing slots [4-6].

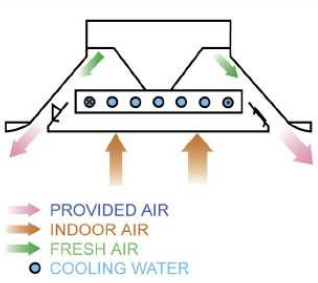

Figure 1. The functional principle of a chilled beam.

2. Modelling

Let consider a confined air volume standing inside a standard room. Physical properties of fluid are reported in Table 1. The standard room transversal section is outlined in Figure 2.

Air physical properties	
Density, ρ	1.19 [kg/m^3]
Dynamic viscosity, η	1.75 e-5 [Pa s]
Specific heat, C_p	1100 [J/(kg K)]
Thermal conductivity, λ	0.026 [W/(m K)]

Table 1: Physical properties assumed for fluid.

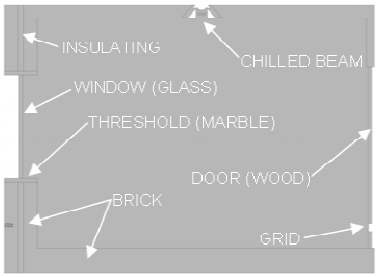

Figure 2. Outline of the studied standard room.

Constituting structural element properties are listed in Table 2.

Properties of solid materials			
Material	ρ [kg/m^3]	C_p [J/(kg K)]	λ [W/(m K)]
Brick	900	830	0.50
Marble	2700	800	2.80
Wood	420	2700	0.12
Insulating	30	1250	0.04
Glass	2500	840	1.00

Table 2: Physical properties for materials.

The chilled beam component for air conditioning is located at the room ceiling. From a fluid-dynamical point of view, governing equations for Newtonian and incompressible fluid modelled by a k-ε turbulent scheme read as in following :

$$\rho\frac{\partial u}{\partial t}+\rho u\cdot\nabla u=\nabla\cdot\left[-pI+(\eta+\eta_T)\left(\nabla u+(\nabla u)\right)^T\right]+F$$

$$\frac{\partial \rho}{\partial t}+\nabla\cdot(\rho u)=0$$

$$\rho\frac{\partial k}{\partial t}+\rho u\cdot\nabla k=\nabla\left[\left(\eta+\frac{\eta_T}{\sigma_k}\right)\nabla k\right]+\eta_T P(u)-\rho\varepsilon$$

$$\rho\frac{\partial \varepsilon}{\partial t}+\rho u\cdot\nabla \varepsilon=\nabla\left[\left(\eta+\frac{\eta_T}{\sigma_\varepsilon}\right)\nabla\varepsilon\right]+\frac{C_{\varepsilon 1}\varepsilon\eta_T P(u)}{k}-\frac{C_{\varepsilon 2}\rho\varepsilon^2}{k}$$

where

$$P(u)=\nabla u:\left(\nabla u+(\nabla u)^T\right) \text{ and } \eta_T=\frac{\rho C_\mu k^2}{\varepsilon}$$

Temperature field can be computed by solving energy conservation equation, reported below:

$$\rho C_p\frac{\partial T}{\partial t}+\nabla\cdot(-k\nabla T)=Q-\rho C_p u\cdot\nabla T$$

The above partial differential equations are numerically integrated with the following fluid-dynamical and thermal boundary conditions:

- No-slip condition at solid walls;
- Velocity imposed (u_{in}) for incoming air through the nozzles of the chilled beam;
- Pressure imposed in correspondence of the recovery grid for air;

- Temperature imposed temperature for incoming air (T_{air});
- Temperature imposed temperature for heat exchanger tube surfaces (T_{batt});
- Convective thermal flux imposed for confining lateral walls: external (T_{ext}, h_{ext}) and internal (T_{int}, h_{int});
- Convective flux through the recovery grid;
- Adiabatic condition for floor and roof.

Differential operators are spatially discretized on non-uniform and non-structured computational grids. Time integration lies on a backward Euler method basing on an implicit time-stepping scheme solving a nonlinear system of equations at each time step. Steady solution is performed by applying a Newton-Raphson method where linear system are solved by an Unsymmetrical Multi-Frontal Package. Computations are carried-out on a 64 bit dual-core workstation disposing of 16 GB of RAM.

Three typologies of active chilled beam are studied. They are geometrically characterized by:

- Vertical disposition both for nozzles of incoming fresh air and heat exchanger tubes;
- Horizontal disposition both for nozzles of incoming fresh air and heat exchanger tubes;
- Inclined (45°) disposition for nozzles of incoming fresh air and horizontal disposition for heat exchanger tubes;

Enlargements of the different systems are reported in Figures 3-5 (an half portion of system for each one), where computational grids are also illustrated.

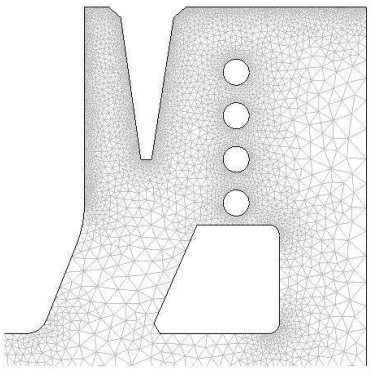

Figure 3. Vertical nozzles and vertical battery.

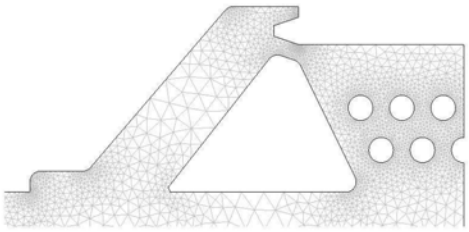

Figure 4. Horizontal nozzles and horizontal battery.

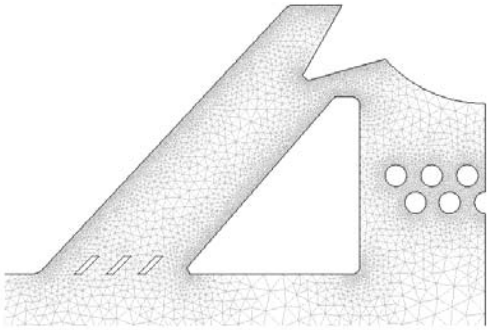

Figure 5. Inclined nozzles and horizontal battery.

The first and the second above cited systems are modelled in 3D also (Figures 6-7). This item allows to study the effect on the air distribution inside the room due to the pressure drops along the adduction ducts of fresh air. Those ducts are presented in Figures 8-9.

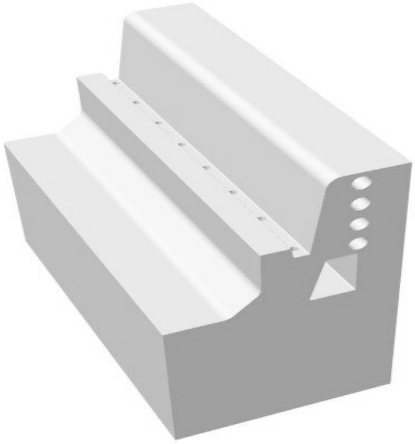

Figure 6. Vertical nozzles and vertical battery.

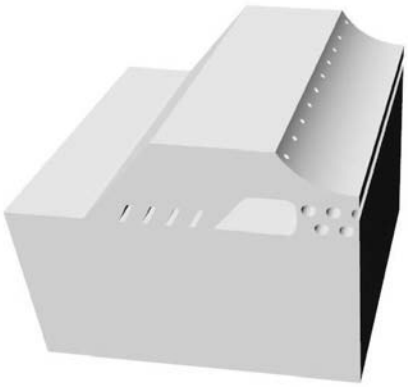

Figure 7. Inclined nozzles and horizontal battery.

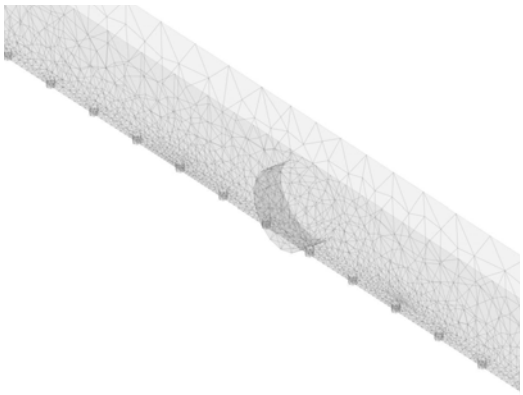

Figure 8. Fresh air adduction channel (system of Figure 6).

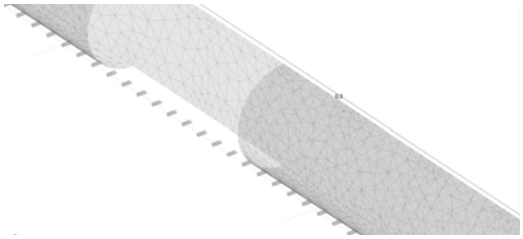

Figure 9. Fresh air adduction channel (system of Figure 7).

3. Results

Results refer to parametric analysis of the studied system (for the above discussed several geometrical configurations of the chilled beams) both in winter and summer climatic conditions. In Table 3 values of parameters, or their range of variation, are reported.

Parameter	winter	summer
T_{ext} [°C]	-5	35
h_{ext} [W/(m^2 K)]	25	25
T_{int} [°C]	8	28
h_{int} [W/(m^2 K)]	8	8
T_{batt} [°C]	40-45	16-21
u_{in} [m/s]	8-20	8-20
T_{air} [°C]	18-22	16-20

Table 3: Values or range of variation for parameters.

In Figure 10 velocity vectors and contour lines for the velocity field drawn for u_{in} assumed 10 [m/s]. In Figures 11 an example of thermal field, referring to summer condition, is plotted.

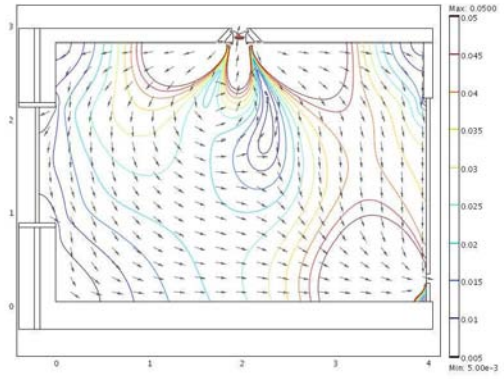

Figure 10. Velocity vectors (normalised) and contour lines (reported values in [m/s]) of the velocity field .

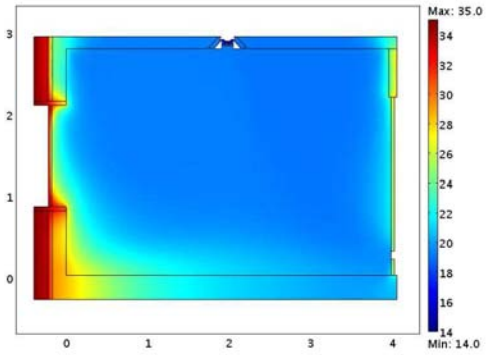

Figure 11. Thermal field (summer conditions).

From analysis of fluid-dynamical and thermal fields some considerations can be globally deduced. The velocity fields computed show an almost constant distribution in the portion of the considered standard room supposed occupied by human presence. Varying the imposed inlet velocity of air flow through the chilled beam nozzles, velocity vectors quantitatively changes closed to the inlet components only. Otherwise, in the main region of the room the almost constant distribution of the dynamical field is detected, characterized by velocity values less then 0.1 [m/s] (Figure 10). Vertical and horizontal temperature gradient, in the portion of the room where people stand, appear slight. This assumption is also supplied by data reported in Figures 12 where temperature values evaluated for height 1.60 [m] from the floor are plotted as function of room width for parametric analyses during summer season ($16°C \leq T_{batt} \leq 20°C$).

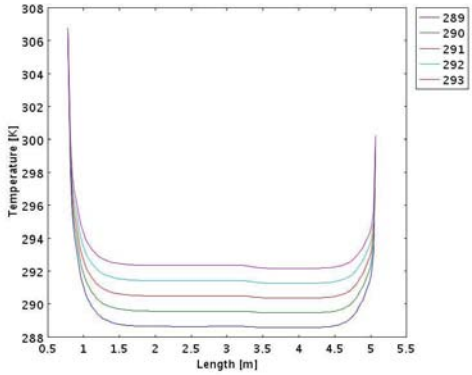

Figure 12. Temperature as function of room width for different temperature of the local heat exchanger (summer).

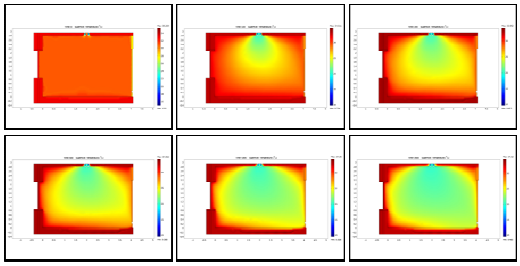

Figure 13. Thermal field during transient analysis for summer climatic conditions.

The above discussed arguments reflect design criteria, usually adopted in project of ventilation and air conditioning systems for buildings, in order to guarantee full comfort indoor conditions for human occupants. The last consideration underlines the potentiality of the numerical

approach in studying this kind of engineering problems.
In Figure 13 computed thermal field during a transient analysis are reported for several time steps. This kind of investigation allows to estimate thermal inertia of the system, due to the combination of geometrical and physical properties of the structural elements of the room and air conditioning system. Chilled beams systems are seen to achieve stationary conditions for air temperature in the occupied region of the room in about 30 minutes since initial time and applying the hardest climatic conditions both in winter and in summer.

Let now consider the functional principle of the active chilled beams with respect to results carried-out in this study. From Figure 14-15 it is clearly deductible as the inlet high velocity jet of fresh air produces a low pressure zone surrounding the nozzle, inducing indoor fluid to flow through the heat exchange battery.

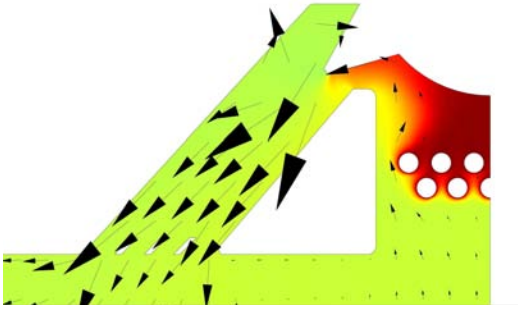

Figure 14. Thermal field and velocity vectors close to the chilled beam (winter).

Figure 15. Thermal field and velocity vectors close to the chilled beam (summer).

A thermal plume characterizing heating or cooling of re-circulated air is observable. In order to quantify the induction effect of the fresh air flow (primary flow) respect to the indoor air flow (secondary flow), the ratio between primary and secondary mass flow rate is evaluated. In Figure 16 results concerning the so computed Induction Ratio (IR %) are reported for several values of imposed inlet velocity of the primary flow.

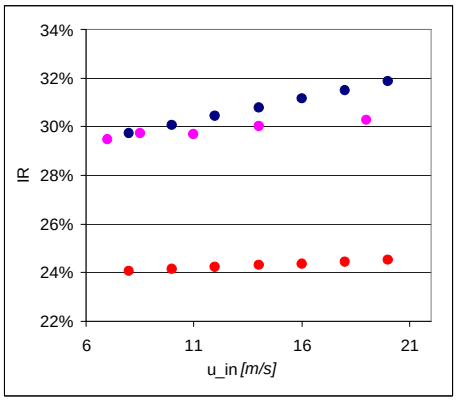

Figure 16. Induction Ratio Vs u_{in} for vertical (blue), horizontal (red) and inclined (magenta) nozzles.

The IR values show a very low sensitivity respect to the inlet velocity imposed for fresh air. The range of variation (24-32%) for the 3 configurations of the chilled beam considered are in good accordance with technical data proposed by the leading constructors of those components. Pressure drop generated by heating/cooling battery crossing is also evaluated. Figure 17 illustrates the computed pressure field for one of the analysed configuration. In Figure 18 pressure drop is reported for the less favourable configuration (45° inclined nozzles, horizontal battery) as a function of u_{in}.

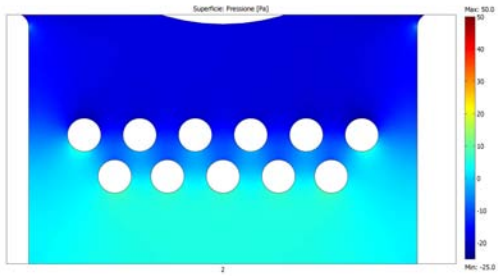

Figure 17. Pressure field close to the heat exchanger.

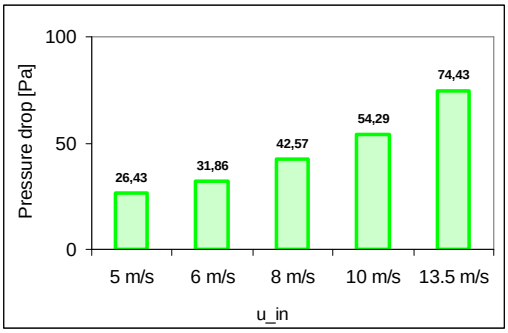

Figure 18. Pressure drop Vs u_{in} (inclined nozzles).

From an applicative point of view, heating/cooling capacity represents the most important parameter characterizing the analyzed components. Heating/cooling capacity is computed from simulations by using the following expression for the primary flow:

$$q = S_{nozzle}\ u_{in}\ \rho\ C_p\ (T_{air} - T_{amb})$$

where S_{nozzle} is the total inlet surface of fresh air for 1 [m] of length (we consider 60 nozzle per meter). Concerning the secondary flow it is assumed:

$$Q = S_{cross}\left(\frac{1}{W_{batt}}\int_{W_{batt}} u\ dx\right)\rho\ C_p\ (T_{batt} - T_{amb})$$

where S_{cross} is the crossing section for fluid flowing through the battery while W_{batt} represents the battery width. The average value of ambient temperature T_{amb} is chosen 20 [°C]. From results it is to notice that contribution of primary flow in thermal capacity is about 5% of the total all over conducted simulations. In Figures 19-20 heating and cooling capacities are diagrammed as function of the battery temperature. These values refer to the 45° inclined nozzles chilled beam that, according to the obtained results, offers the lower thermal performance than the other configurations. It is to notice that, during summer season, a better thermal performance obtained decreasing battery temperature is limited by the condensation risk on tube surfaces standing on the room ceiling. Influence of pressure drop in adduction channels of fresh air on the Induction Ratio is also investigated by 3D simulations.

Computing procedure is divided into two steps. Firstly dynamical fields are solved in adduction channel domains, then computed outgoing velocity in nozzles cross sections are used as boundary conditions for solving 3D models of the chilled beams (Figures 21-22). Despite of a non-uniform distribution of velocity over the nozzles, the IR results very slightly influenced.

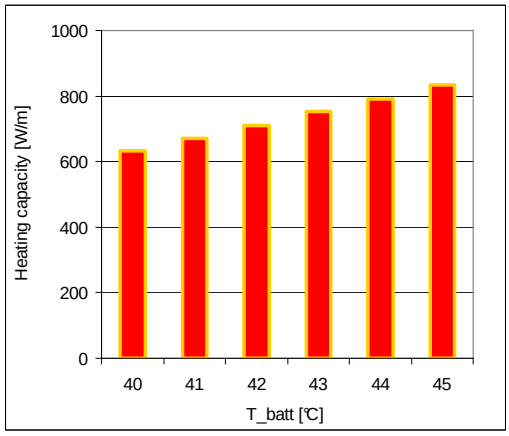

Figure 19. Heating capacity Vs T_{batt} (winter).

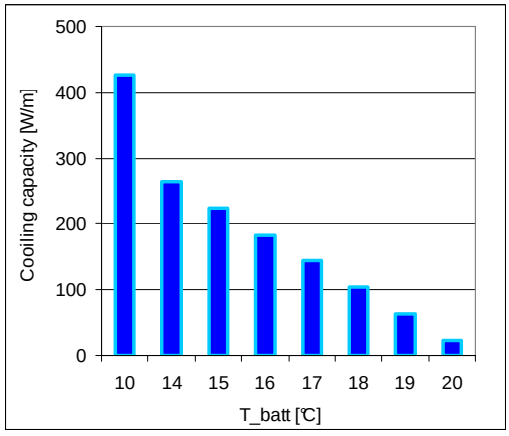

Figure 20. Cooling capacity Vs T_{batt} (summer).

4. Conclusions

A numerical study for evaluating fluid-dynamical and thermal performance of chilled beams for air conditioning systems is conducted by exploiting COMSOL Multiphysics. Two- and

three-dimensional models are built for three typologies of the considered technological system. Computations are carried-out for steady and transient analysis, simulating both summer and winter functioning and varying some typical operating conditions for those components. Two main parameters are analysed for investigating on dynamical and thermal efficiency: the Induction Rate and the thermal capacity. Indoor comfort conditions are also investigated for a chosen standard room.

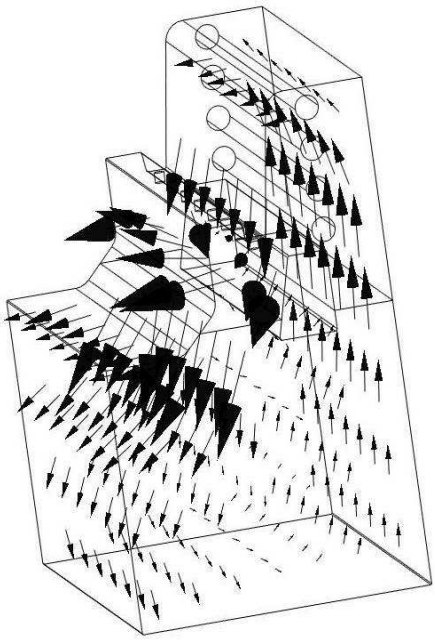

Figure 21. Velocity vectors.

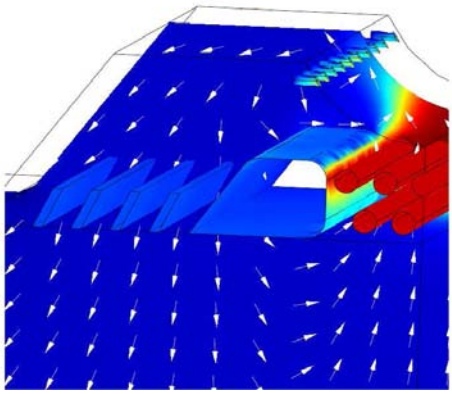

Figure 22. Thermal field (winter).

Results show a good correspondence with indications supplied by technical sheets of leading constructors of this components. This study highlights the opportunity of CFD approach both in design of ventilation and air conditioning components and in their specific application concerning room geometry and thermal load.

5. References

1. F. Alamari, D.J.G. Butler, P.F. Grigg and M.R. Shaw, Chilled ceilings and displacement ventilation, *Renewable Energy*, **15,** 300-305 (1998)

2. J. Fredriksson, M. Sandberg, B. Moshfegh, Experimental investigation of the velocity field and airflow pattern generated by cooling ceiling beams, *Building and environment*, **36,** 891-899 (2001)

3. S.J. Rees, J.J. McGuirk, P. Haves, Numerical investigation of transient buoyant flow in a room with a displacement ventilation and chilled ceiling system, *International Journal of Heat and Mass transfer*, **44,** 3067-3080 (2001)

4. A. Novoselac, J. Srebric, A critical on the performance and design of combinated cooled ceiling and displacement ventilation systems, *Energy and Buildings*, **34,** 497-509 (2002)

5. X. Hao, G. Zhang, Y. Chen, S. Zou; D. J. Moschandreas, A combined system of chilled ceiling, displacement ventilation and desiccant dehumidification, *Building and Environment*, **42,** 3298-3308 (2007)

6. Hazim B. Awbi, *Ventilation of buildings*, Taylor & Francis, London (1991)